Thermoelectric mesoscopic phenomena / Phénomènes thermoélectriques mésoscopiques

Thermoelectric transport and Peltier cooling of cold atomic gases

Transport themoélectrique et refroidissement Peltier dans des gaz d'atomes froids

Charles Grenier [a], Corinna Kollath [b], Antoine Georges [c,d,e,∗]

[a] *Laboratoire de physique, ENS de Lyon, Université de Lyon, CNRS, 46, allée d'Italie, 69364 Lyon, France*
[b] *HISKP, University of Bonn, Nussallee 14–16, 53115 Bonn, Germany*
[c] *Collège de France, 11, place Marcelin-Berthelot, 75005 Paris, France*
[d] *Centre de physique théorique, École polytechnique, CNRS, Université Paris-Saclay, 91128 Palaiseau, France*
[e] *DQMP, Université de Genève, CH-1211 Genève, Switzerland*

A R T I C L E   I N F O

A B S T R A C T

This brief review presents the emerging field of mesoscopic physics with cold atoms, with an emphasis on thermal and 'thermoelectric' transport, i.e. coupled transport of particles and entropy. We review in particular the comparison between theoretically predicted and experimentally observed thermoelectric effects in such systems. We also show how combining well-designed transport properties and evaporative cooling leads to an equivalent of the Peltier effect with cold atoms, which can be used as a new cooling procedure with improved cooling power and efficiency compared to the evaporative cooling currently used in atomic gases. This could lead to a new generation of experiments probing strong correlation effects of ultracold fermionic atoms at low temperatures.

R É S U M É

Cette courte revue présente le domaine émergent de la physique mésoscopique avec les atomes froids, et met l'accent sur le transport thermique et « thermoélectrique », c'est-à-dire le transport couplé de particules et d'entropie. Nous comparons notamment des prédictions théoriques à des observations expérimentales d'effets thermoélectriques au sein de ces systèmes. Nous montrons aussi comment la combinaison de propriétés de transport bien adaptées et du refroidissement évaporatif conduit à l'équivalent d'un effet Peltier pour atomes froids, pouvant fournir une nouvelle méthode de refroidissement présentant un rendement et une puissance améliorés en comparaison du refroidissement évaporatif usuellement utilisé dans les gaz d'atomes froids. Ceci pourrait conduire à une nouvelle

génération d'expériences permettant de sonder les effets de corrélations fortes dans les gaz d'atomes fermioniques ultra-froids aux basses températures.

1. Introduction

The last fifteen years have established ultracold atomic gases as efficient quantum simulators [1–4]. Using those extremely flexible systems in which geometry, interactions and disorder can be tuned at will, experiments on synthetic materials have been performed. These experiments reveal the characteristics of various phase transitions, and contribute to our understanding of strongly correlated matter.

From this perspective, it is then quite natural to explore whether this potential for quantum simulation can be extended to out-of-equilibrium properties, such as transport, dissipation or thermalization in quantum systems. In recent years, numerous experiments and theory proposals have emerged, making cold atom transport a very active field: owing to the flexibility of cold atomic setups, many different configurations have been realized [5–13], which are as many different probes of the out-of-equilibrium properties of quantum systems. In parallel, a whole branch of research in cold atoms is now devoted to the realization of circuits in which Bose–Einstein condensates replace electrons [14,15], thus founding the field of atomtronics [16,17].

A similar line of thought is to extend the idea of quantum simulation to two terminal transport setups made of cold atoms [18,19,7,20,21]. This has recently brought transport experiments into new regimes thanks to the control on interactions [22,23] with Feshbach resonances. This allows one to address fundamental questions of mesoscopic physics, such as the interplay between interactions and disorder [24,25], or quantized conductance and interactions [26].

Of great interest in this context is thermal transport (i.e. the transport of entropy), as well as the combined transport of entropy and particles. We shall loosely refer to the latter as 'thermoelectric' transport, in line with standard condensed matter terminology, notwithstanding that in the present context we are dealing with neutral atoms.

Combining the flexibility and cleanliness of cold atom systems and the nice transport features of mesoscopic devices is particularly exciting, and provides an avenue to improve our understanding of thermal and thermoelectric transport. Such investigations on clean and controllable systems might also prove helpful to propose systematic guidelines to build new materials with interesting transport properties, which can be envisioned for energy saving purposes, for example. In return, one may expect that the methods developed in mesoscopic physics might be helpful to tackle some of the outstanding problems in cold atom physics, such as cooling.

This brief review is organized as follows: in section 2, we discuss thermoelectric effects for cold atoms. We introduce our theoretical description and compare the obtained results with experimental data obtained in the quantum optics group at ETH Zürich. Then, we show how using a combination of evaporative cooling and well designed transport properties can lead to a better cooling procedure which has a high efficiency and can reach low temperatures, thus proposing a solution to a long-standing problem in the cold atom community.

2. Thermoelectricity with neutral particles

This section discusses a theory experiment comparison on thermal and thermoelectric effects concentrating on fermionic atoms [27], based on a theory proposal exposed in [28]. A bosonic counterpart of those results exist both on the experimental [29] and theoretical [30] sides. Thermoelectric effects are fundamental probes for materials and investigating them in controlled and flexible systems such as cold atoms is a good opportunity to understand better the necessary ingredients to improve the thermoelectric figure of merit or power-factor [31]. Here, we discuss the model that has been compared to experimental results obtained at ETH. In particular, we show how the magnitude of thermoelectric effects and the efficiency of energy conversion can be optimized by controlling the geometry (in the ballistic regime) or the disorder strength in the junction. By investigating systematically the ballistic-diffusive crossover as a function of disorder, we also illustrate clearly that thermopower and conductance measurements are complementary probes of the transport properties of a given system.

We point out that the setup is a good test-bed for investigating the thermodynamics of small systems, by demonstrating its potential to explore the mechanisms of energy conversion from heat to chemical energy.

2.1. Basics of cold atom thermoelectricity

2.1.1. Model

The setup under consideration is the two-terminal setup sketched in Fig. 1. The setup is largely inspired by the ubiquitous Landauer configuration of mesoscopic physics [32,33]. A large atomic cloud is divided by a suitable laser beam into two reservoirs which are connected by a narrow channel. A detailed description of the setup can be found in [18].

The junction between the two reservoirs can be considered as a circuit element having a conductance G, a thermal conductance G_T and a thermopower α_{ch}. In order to get a key signature of thermoelectric effects, the reservoirs are prepared
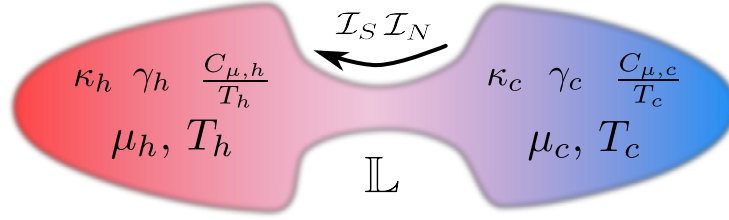
Fig. 1. Setup for thermoelectricity (sketch). The two reservoirs (h for hot, c for cold) exchange particles and heat through a junction characterized by its linear response properties represented by the matrix $\mathbb{L}$ defined in the main text. The thermodynamic response of each reservoir is represented by the coefficients κ, γ and C_N, which denote respectively the compressibility, the dilatation coefficient and the heat capacity at constant particle number (see text).

with N atoms each at a temperature T. Then, one side is heated up to a temperature $T_h = T + \Delta T_0$, the populations of the two reservoirs remaining the same.

Cold atom systems are well isolated. This means in particular that the total particle number is conserved, implying that current between the reservoirs is only a transient effect and no stationary regime will be reached. It is useful to view the above setup as the analogue of a capacitor (each plate being a reservoir) connected to a resistor (representing the junction), and the actual experiment as the transient discharge of this capacitor.

We assume that the temperature and chemical potential biases $\Delta T = T_h - T_c$ and $\Delta \mu = \mu_h - \mu_c$ are small with respect to the Fermi temperature T_F and energy E_F (with $T_F = E_F/k_B$) of the entire cloud. Therefore, particles and heat flow can be described using linear response and the transport properties of the junction by a constant matrix $\mathbb{L}$ of transport coefficients.

Thermoelectric effects originate from a reversible coupling between heat and particle flows [34,31]. Within linear response, the expressions of the particle and entropy currents $\mathcal{I}_N$ and $\mathcal{I}_S$ in terms of the chemical potential and temperature biases $\Delta \mu$ and ΔT are obtained following Onsager's picture of coupled transport processes [35,36]:

$$\begin{pmatrix} \mathcal{I}_N \\ \mathcal{I}_S \end{pmatrix} = \frac{d}{dt} \begin{pmatrix} N_h - N_c \\ S_h - S_c \end{pmatrix} = -\mathbb{L} \begin{pmatrix} \Delta \mu \\ \Delta T \end{pmatrix} \quad \mathbb{L} = G \begin{pmatrix} 1 & \alpha_{ch} \\ \alpha_{ch} & \mathcal{L} + \alpha_{ch}^2 \end{pmatrix} \tag{1}$$

where G and α_{ch} are the conductance and thermopower of the junction, respectively, and $\mathcal{L} = \frac{G_T}{TG}$ is the Lorenz number of the junction, with G_T the thermal conductance.[1] Note that, in the present context of neutral particles, G, α_{ch}, G_T/T and $\mathcal{L}$ have the dimensions of $1/h$, k_B, k_B^2/h and k_B^2, respectively, with h the Planck constant and k_B the Boltzmann constant.

For usual (*electronic*) condensed matter systems, the (electro)chemical potential and temperature differences at the boundaries of the circuit element are imposed through metallic reservoirs. This is a major difference with cold atomic systems, which are intrinsically isolated, and are thus described in the microcanonical ensemble. Experimentally, this feature translates into the application of a particle number and entropy imbalance between the two reservoirs, instead of a combined chemical potential and temperature imbalance. Taking this into account requires to relate the chemical potential and temperature differences to the population and entropy imbalances at any time. Under the assumption of a quasistatic evolution,[2] ΔN and ΔS are related to $\Delta \mu$ and ΔT through the following set of thermodynamic relations:

$$\begin{pmatrix} \Delta N \\ \Delta S \end{pmatrix} = \mathbb{K} \cdot \begin{pmatrix} \Delta \mu \\ \Delta T \end{pmatrix} = \kappa \begin{pmatrix} 1 & \gamma \\ \gamma & \ell + \gamma^2 \end{pmatrix} \cdot \begin{pmatrix} \Delta \mu \\ \Delta T \end{pmatrix} \tag{2}$$

which define the linear thermodynamic response of the reservoirs. The relations (2) have been cast in a form that is very similar to that of the linear transport equations (1), except that thermodynamic coefficients instead of transport coefficients are involved here. In this expression, $\kappa = \frac{\partial N}{\partial \mu}|_T$ is the compressibility, $\gamma = \frac{1}{\kappa} \cdot \frac{\partial N}{\partial T}|_\mu = \frac{1}{\kappa} \cdot \frac{\partial S}{\partial \mu}|_T$ is a dilatation coefficient measuring the variation of the particle number with temperature,[3] and ℓ is a thermodynamic analogue of the Lorenz number for the reservoirs. It can be easily shown that $\ell = \frac{C_N}{T\kappa}$, with C_N the specific heat at constant particle number.

The exact expression of the thermodynamic coefficients is extracted from the equation of state of the gas in the reservoirs. As for the transport properties of the junction, Eq. (2) assumes that the chemical potential and temperature biases are rather small compared to E_F and T_F. As discussed in the supplementary material of [27], this linear response approximation is surprisingly robust. In addition, the reference thermodynamic equilibrium state in which the matrices $\mathbb{K}$ and $\mathbb{L}$ should be computed is the final one, in which both reservoirs have the same particle number $\bar{N} = \frac{N_{tot}}{2}$ and temperature $\bar{T} = T + \frac{\Delta T_0}{2}$, and consequently have the same chemical potential $\bar{\mu}$.

The thermodynamic coefficients appearing in (2) are given by the following formulae, with the density of states of a harmonically trapped, noninteracting gas $g(\varepsilon) = \frac{\varepsilon^2}{4(\hbar\omega_x \hbar\omega_y \hbar\omega_z)}$:

---

[1] Thermoelectric effects are usually described with the heat current instead of the entropy current, which we keep here for symmetry reasons.

[2] Experimentally, data points are acquired approximately every 100 ms, a time longer than the thermalization time in the reservoirs, expected to be around 10 ms.

[3] One also has $\gamma = -\frac{\partial \mu}{\partial T}$ at constant particle number.

$$\kappa = \int_0^\infty d\varepsilon\, g(\varepsilon) \left(-\frac{\partial f}{\partial \varepsilon} \right) \tag{3}$$

$$T\gamma\kappa = \int_0^\infty d\varepsilon\, g(\varepsilon)\, (\varepsilon - \mu) \left(-\frac{\partial f}{\partial \varepsilon} \right) \tag{4}$$

$$\frac{C_N}{T} + \kappa\gamma^2 = \int_0^\infty d\varepsilon\, g(\varepsilon)\, (\varepsilon - \mu)^2 \left(-\frac{\partial f}{\partial \varepsilon} \right) \tag{5}$$

where $f(\varepsilon) = \frac{1}{1+e^{\beta(\epsilon - \mu)}}$ is the Fermi–Dirac distribution. The response of the reservoirs to the temperature and particle number imbalance is assumed to be independent of the transport properties of the junction, in analogy with the junction/reservoir separation in the Landauer picture of mesoscopic transport.

2.1.2. Theoretical results and predictions

Combining the equations (1) and (2) gives the following equation ruling the time evolution of the population and temperature imbalances:

$$\tau_0 \frac{d}{dt} \begin{pmatrix} \Delta N \\ \Delta T \end{pmatrix} = - \begin{pmatrix} 1 & \kappa\alpha \\ \frac{\alpha}{\ell\kappa} & \frac{\mathcal{L}+\alpha^2}{\ell} \end{pmatrix} \cdot \begin{pmatrix} \Delta N \\ \Delta T \end{pmatrix} \tag{6}$$

where the global timescale $\tau_0 = \kappa/G$ has been identified and measured in [18] and $\alpha = \alpha_{\mathrm{ch}} - \gamma$ is the total thermopower of the system. This last relation shows in particular that the coupled particle and heat transport properties of the total system arise as a competition between the thermal expansion of the reservoirs represented by γ and the thermopower of the junction represented by α_{ch}. Those two coefficients represent two different mechanisms for entropy transport: γ accounts for the entropy cost associated with the displacement of a particle from one reservoir to the other, and α_{ch} is directly identified as the amount of entropy carried by each particle entering the junction. Integrating (6) provides the time dependence of the population and temperature differences, with ΔN_0 and ΔT_0 the initial population and temperature imbalance, respectively.

The general solution to the evolution equations (6), given an initial particle and temperature difference ΔN_0 and ΔT_0, reads[4]:

$$\Delta N(t) = \left\{ \frac{1}{2} \left[e^{-t/\tau_-} + e^{-t/\tau_+} \right] + \left[1 + \frac{\mathcal{L}+\alpha^2}{\ell} \right] \frac{e^{-t/\tau_-} - e^{-t/\tau_+}}{2(\lambda_+ - \lambda_-)} \right\} \Delta N_0 + \frac{\alpha\kappa}{\lambda_+ - \lambda_-} \left[e^{-t/\tau_-} - e^{-t/\tau_+} \right] \Delta T_0 \tag{7}$$

$$\Delta T(t) = \left\{ \frac{1}{2} \left[e^{-t/\tau_-} + e^{-t/\tau_+} \right] - \left[\frac{\mathcal{L}+\alpha^2}{\ell} - 1 \right] \frac{e^{-t/\tau_-} - e^{-t/\tau_+}}{2(\lambda_+ - \lambda_-)} \right\} \Delta T_0 + \frac{\alpha}{\ell\kappa(\lambda_+ - \lambda_-)} \left[e^{-t/\tau_-} - e^{-t/\tau_+} \right] \Delta N_0 \tag{8}$$

The inverse timescales $\tau_\pm^{-1} = \tau_0^{-1}\lambda_\pm$ are given by the eigenvalues of the transport matrix:

$$\lambda_\pm = \frac{1}{2}\left(1 + \frac{\mathcal{L}+\alpha^2}{\ell} \right) \pm \sqrt{\frac{\alpha 2}{\ell} + \left(\frac{1}{2} - \frac{\mathcal{L}+\alpha^2}{2\ell} \right)^2} \tag{9}$$

These equations can be viewed as ruling the discharge dynamics of a thermoelectric capacitor.

The channel is modeled by a linear circuit element at the average temperature $\bar{T}$ and chemical potential $\bar{\mu}$. Its linear transport coefficients are given by the following expressions, which have a form very similar to those of the thermodynamic coefficients in equations (3), (4) and (5):

$$G = \frac{1}{h} \int_0^\infty d\varepsilon\, \Phi(\varepsilon) \left(-\frac{\partial f}{\partial \varepsilon} \right) \tag{10}$$

$$T\alpha_{\mathrm{ch}}G = \frac{1}{h} \int_0^\infty d\varepsilon\, \Phi(\varepsilon)\, (\varepsilon - \mu) \left(-\frac{\partial f}{\partial \varepsilon} \right) \tag{11}$$

$$\frac{G_T}{T} + G\alpha_{\mathrm{ch}}^2 = \frac{1}{h} \int_0^\infty d\varepsilon\, \Phi(\varepsilon)\, (\varepsilon - \mu)^2 \left(-\frac{\partial f}{\partial \varepsilon} \right) \tag{12}$$

---

[4] The expressions provided in the supplementary information of [27] contains typographical errors, that have been corrected here.

where $\Phi(\varepsilon)$ is the transport function of the channel. Note the formal similarity with the above equations for the thermodynamic coefficients of the reservoirs, with here the transport function playing the role of the density of states. A simple interpretation of $\Phi(\varepsilon)$ is the number of channels available for a particle having an energy ε [32], since at zero-temperature $G(T = 0) = \Phi(E_F)/h$. In the case of a single channel, the transport function reduces to the transmission probability as a function of energy. More generally, for noninteracting particles of mass M propagating along the y-direction and harmonically confined in the transverse (x, z) direction, the transport function reads:

$$\Phi(\varepsilon) = \sum_{n_z=0}^{\infty} \sum_{n_x=0}^{\infty} \int_0^{\infty} dk_y \frac{\hbar k_y}{M} \mathcal{T}(k_y) \delta \left(\varepsilon - \hbar\omega_x(n_x + 1/2) - \hbar\omega_z(n_z + 1/2) - \frac{\hbar^2 k_y^2}{2M} \right) \tag{13}$$

$$= \sum_{n_z=0}^{\infty} \sum_{n_x=0}^{\infty} \mathcal{T}(\varepsilon - \hbar\omega_x(n_x + 1/2) - \hbar\omega_z(n_z + 1/2)) \vartheta (\varepsilon - \hbar\omega_x(n_x + 1/2) - \hbar\omega_z(n_z + 1/2)) \tag{14}$$

where $\mathcal{T}$ is the transmission probability.[5] The difference between the various transport regimes is contained in the transmission probability $\mathcal{T}$. In (13), the energy conservation condition states that a particle entering the channel will distribute its energy between kinetic (propagation with a certain momentum along y) and confinement (populating a transverse mode along x and z).

The energy dependence of the transport function Φ close to the chemical potential creates a particle-hole asymmetry which enhances the value of the thermopower α_{ch}. This effect is larger when the energy dependence is stronger, as is the case when the conduction regime goes from ballistic to diffusive, or when the confinement increases. This can be understood by applying a Sommerfeld expansion to the formulae (3), (4), (10) and (11), giving the following result for the total thermopower of the combined junction and reservoirs system[6]:

$$\alpha = \frac{\pi^2 k_B^2 T}{3} \left[\frac{\Phi'(E_F)}{\Phi(E_F)} - \frac{g'(E_F)}{g(E_F)} \right] \tag{15}$$

where E_F is the common Fermi energy of the system at equilibrium, and Φ' (resp. g') the energy derivative of Φ (resp. g). The first lesson of this formula is that the thermopower vanishes at low T, in agreement with the low temperature behavior of entropy. Also, at high temperature when the Fermi function in the expression of the transport coefficients can be replaced by a Boltzmann distribution, we see that $\alpha \propto 1/T$. These considerations imply qualitatively that thermoelectric effects are expected to be maximal around the Fermi temperature.

For a ballistic junction, when $E_F \gg \hbar\omega_{i,ch}$, where $\omega_{i,ch}$ are the transverse confinement energies in the junction, implying that the number of channels is sufficiently large, the total thermopower can be approximated by the following expression:

$$\alpha_{\text{Ballistic}} = \frac{2\pi^2 k_B^2 T}{3} \left[\frac{1}{E_F - \frac{\hbar\omega_{x,ch} + \hbar\omega_{z,ch}}{2}} - \frac{1}{E_F - \frac{\hbar\omega_{x,r} + \hbar\omega_{z,r}}{2}} \right] \tag{16}$$

The confinement frequencies $\omega_{i,ch}$ are significantly bigger than those in the reservoirs $\omega_{i,r}$, implying that the first term (the thermopower of the junction) is dominating in (16) over the contribution of the reservoirs.

For a diffusive junction in which $E_F \gg \hbar\omega_{i,ch}$, the total thermopower reads in the constant scattering time approximation [37]:

$$\alpha_{\text{Diffusive}} = \frac{\pi^2 k_B^2 T}{3} \left[\frac{5/2}{E_F - \frac{\hbar\omega_{x,ch} + \hbar\omega_{z,ch}}{2}} - \frac{2}{E_F - \frac{\hbar\omega_{x,r} + \hbar\omega_{z,r}}{2}} \right] \tag{17}$$

showing that thermoelectric effects are expected to be easier to observe, owing to the stronger energy dependence of the transport function Φ. A systematic comparison of those predictions to experimental data acquired in the ballistic-diffusive crossover will be discussed in the following section.

Entering the quantum regime of conduction has also interesting consequences on thermopower, which are known as nanostructuration in the context of mesoscopic physics. For a junction with transverse modes having energies ε_{n_x,n_z}, thermopower reads:

$$\alpha_{ch} = k_B \frac{\sum_{n_x,n_z \geq 0} \left(\xi_{n_x,n_z} - \xi \right) f(\varepsilon_{n_x,n_z}) + \log\left[1 + e^{\xi - \xi_{n_x,n_z}}\right]}{\sum_{n_x,n_z \geq 0} f(\varepsilon_{n_x,n_z})} \tag{18}$$

with $\xi = \beta\mu$ and $\xi_{n_x,n_z} = \beta\varepsilon_{n_x,n_z}$. As depicted in Fig. 2a), this expression for thermopower leads to oscillations as a function of the trapping frequency: negative values correspond to a reservoir-dominated thermoelectric transport, where particles

---

[5] Strictly speaking, the transmission probability depends on momentum along the translationary invariant direction, but it is commonly defined as an energy dependent quantity without loss of generality.

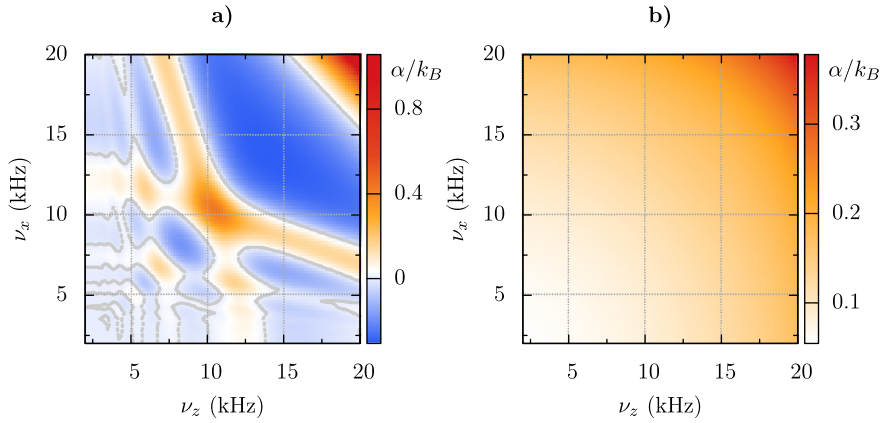[6] This result is known as the Mott–Cutler formula for thermopower.

Fig. 2. Nanostructuration with cold atoms. The colors indicate the total thermopower α as a function of the transverse confinement frequencies ν_x and ν_z in the channel, for a fixed Fermi temperature $T_F = 1$ μK. **a)** At low temperature $T/T_F = 0.05$, oscillations are visible. Gray lines indicate vanishing total thermopower. **b)** At high temperature $T/T_F = 0.3$, the oscillations are washed out.

flow from the cold side to the hot one, according to the chemical potential difference, and positive values to a regime in which the channel dominates, as in the experiments described below. Similar oscillations having their origin in the successive opening of new conduction channels have been predicted and observed in quantum point contacts [38]. These oscillations in thermopower as a function of confinement illustrate in a very clear way the nanostructuration ideas proposed by Hicks and Dresselhaus [39,40] more than twenty years ago, and they tend to disappear at higher temperature, as shown in Fig. 2b). When T/T_F is sufficiently large, only the overall increase in amplitude remains visible, as observed in the experiment discussed in the following section.

2.2. Thermoelectric signature

The forthcoming paragraphs will compare the theoretical predictions obtained by the transport equations (21) and (22) to experimental data. The situation we consider is the creation of a temperature imbalance between the two reservoirs. Experimentally, this has been achieved by preparing the two reservoirs with the same number of atoms in both reservoirs and then heating one of them while the junction is closed [27]. First, we will investigate transport through a ballistic junction. Then, we apply a disordered speckle pattern, which changes the properties of the junction to a diffusive junction. In particular, we will consider thermoelectric manifestations and illustrate the complementarity of resistance and thermopower measurements.

2.2.1. First signature of thermoelectric effects and the ballistic regime

Typical time evolutions of the temperature and population imbalances for a ballistic junction are displayed in Fig. 3a and b, respectively. In these figures, the experimental results [27] are compared to the solutions (7) and (8) of the transport equations, both obtained for a Fermi temperature $T_F \simeq 1$ μK and a temperature of $0.35 T_F$.

Two main effects occur. The first one is the exponentially fast equilibration of the temperatures (Fig. 3a) in the two reservoirs, which are initially strongly imbalanced. The second one is that even though initially the particle number is almost balanced in the reservoirs, a transient particle imbalance is induced. Since the hot reservoir has expanded during the heating process in its trap and is thus less dense, naively, one expects a flow from the cold reservoir to the hot one. In other words, a chemical potential imbalance in the reservoirs is introduced, since by heating the chemical potential decreases, which would induce a current from the cold reservoir to the hot one. However, as one can see in Fig. 3b, a flow from the hot reservoir to the cold one occurs at initial times. This counterintuitive direction of the flow is a direct consequence of the thermoelectric coupling in the junction, which overwhelms the effect from the reservoirs. The particle imbalance reaches a maximum when the typical equilibration timescale of the temperature has been reached. Afterwards, a slow equilibration of the particle imbalance takes place to restore thermodynamic equilibrium.

In the ballistic regime, the transverse confinement frequencies can be employed in order to tune the transport properties of the junction. The effect of the confinement in the z direction on the thermoelectric response is displayed in Fig. 3c–d. For a larger trapping frequency ν_z, a larger induced particle number imbalance can be seen, showing that the maximal thermoelectric response $\mathcal{R}$ increases with the trapping frequency ν_z. In both cases, the comparison of the theoretical results for the induced particle imbalance and the experimental measurements is very good.

The increased thermoelectric response with the larger trapping frequency can be understood from a simple estimate (16) of the total thermopower. Computing the derivative of α with respect to one of the confinement frequencies in the channel gives $\frac{\partial \alpha}{\partial \omega_{i,ch}} = \frac{\hbar \pi^2 k_B^2 T}{3} \frac{1}{\left(E_F - \frac{\hbar \omega_{x,ch} + \hbar \omega_{z,ch}}{2} \right)^2} > 0$. This implies that the thermoelectric coupling increases with the confinement in
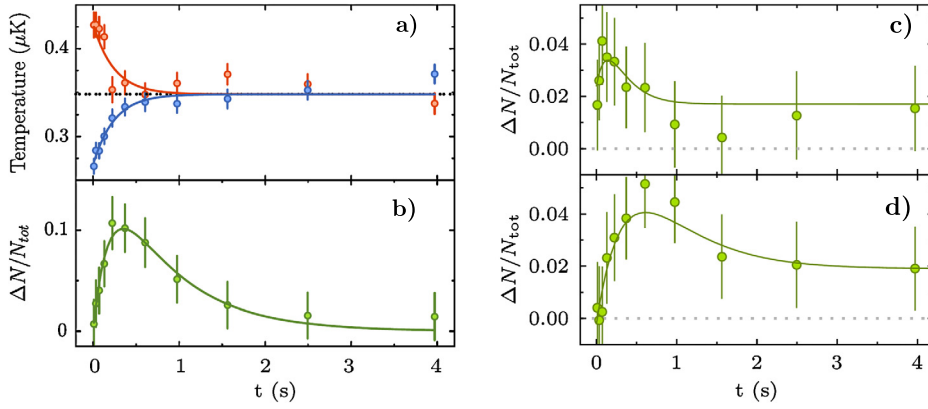
Fig. 3. Temperature and population imbalances, adapted from [27]. **a)** Temperature evolution: T_h (red) and T_c (blue) as a function of time for $\nu_z = 3.5$ kHz and a disorder of average strength 542 nK (see main text). Dashed line: $\bar{T}$ at the initial time. The average temperature does not evolve significantly with time, in agreement with linear response. **b)** Population relative imbalance $\Delta N/N_{tot}$ as a function of time for a disordered channel in which ν_z was set to 3.5 kHz with a disorder of average strength 542 nK (see main text). **c)** and **d)** Time evolution of $\Delta N/N_{tot}$ a ballistic channel with $\nu_z = 3.5$ kHz (**c**) and $\nu_z = 9.3$ kHz (**d**).

the junction, in agreement with the experimental observations. Nevertheless, the effect in this ballistic regime remains hard to observe, and can barely be distinguished from the error bars.

2.2.2. Tuning thermoelectric effects: from ballistic to diffusive junctions

Projecting a disordered potential onto the junction, and thus reaching the diffusive regime, appears as a possibility to improve the junction's thermopower. We consider again the situation in which an initial temperature imbalance is imprinted onto the junction.

The microscopic description of the disordered junction is very involved. Thus, we base our theoretical interpretation of the ballistic-diffusive crossover on a phenomenological transparency $\mathcal{T}$. This transparency $\mathcal{T}$ depends on the energy ε of incident particles, and on the typical height $\bar{V}$ of the disorder potential:

$$\mathcal{T}(\varepsilon, \bar{V}) = \frac{l(\varepsilon, \bar{V})}{l(\varepsilon, \bar{V}) + L} = \frac{v(\varepsilon)\,\tau(\varepsilon, \bar{V})}{v(\varepsilon)\,\tau(\varepsilon, \bar{V}) + L} \tag{19}$$

In (19), l is the mean free path, $v(\varepsilon) = \frac{\hbar k(\varepsilon)}{M}$ is the velocity of the carriers, L is the junction's length and τ is the scattering time. The expression (19) tends to one when the mean free path $l(\varepsilon, \bar{V})$ becomes larger than L, as required in the ballistic regime. When the disorder strength becomes large, $l(\varepsilon, \bar{V}) \ll L$, the transport function reduces to that obtained in the Drude model describing ohmic conduction [37]. We assume that the dominant dependence of the scattering time stems from the speckle power with the form $\tau \propto \bar{V}^B$ and that its energy dependence can be neglected (a common approximation in solid-state systems). In this situation, thermopower is independent of the values of disorder [37].

The results displayed in Fig. 4a show that the presence of a disorder speckle potential in the junction has two effects: first, with increasing disorder strength, the typical transport timescale τ_0 increases, since the resistance of the junction increases. The value of τ_0 can be obtained through a fit of the population and temperature imbalance with the solution to the evolution equation (6). Secondly, disorder leads to an increase in the thermoelectric response directly observed in the time evolution of the population imbalance. A measure for this increase is the thermoelectric response $\mathcal{R}(t) = \frac{\Delta N(t)/N}{\Delta T_0}$, which removes the initial temperature dependence. A particular insight gives the maximal thermoelectric response $\mathcal{R}_{max}$. This quantity is directly proportional to the Seebeck coefficient, and thus characterizes the strength of thermoelectric effects.

Fig. 4b summarizes this information by comparing the increase of the timescale τ_0 and of R_{max} versus the height of the speckle potential. The rise of the timescale τ_0 and of R_{max} imply that the resistance and the Seebeck coefficient of the junction increase with disorder. The resistance essentially increases with disorder and confinement, whereas the thermoelectric response first increases and then saturates in the diffusive regime. This different behavior is exhibited in Fig. 4c, where R_{max} is shown versus the timescale τ_0. The saturation of the thermoelectric response validates the energy-independent relaxation time approximation. This last feature results, at strong disorder, in a scaling of the time-dependent thermoelectric response displayed in Fig. 4d as a function of the dimensionless time t/τ_0. In addition, the different behaviors of τ_0 and $\mathcal{R}_{max}$ clearly show that resistance and thermopower are independent properties describing the transport in the junction.

2.2.3. An ultracold heat engine

From the thermodynamic point of view, the discussed protocol performs a heat-to-current conversion from the initial temperature imbalance to the time-dependent (transient) particle current. The thermodynamic cycle performed in the N–μ plane by this cold atom heat engine is depicted in Fig. 5a: its center signals the final equilibrium, where the conversion
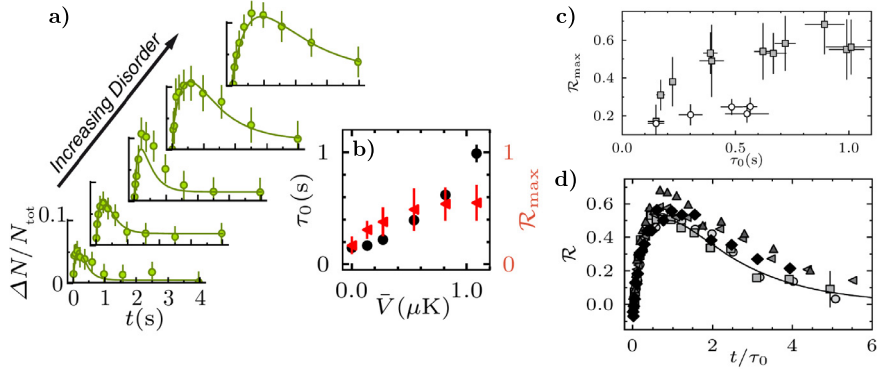
Fig. 4. Ballistic-diffusive crossover, adapted from [27]. **a):** Time evolution of $\Delta N/N_{\text{tot}}$ for a fixed confinement of $\nu_z = 3.5$ kHz across the ballistic-diffusive crossover, with increasing disorder strength ($\bar{V} = 0.14, 0.27, 0.54, 0.81$ and 1.08 μK from bottom to top). Solid lines: theory obtained with the transparency in Eq. (19). **b):** Fitted timescale τ_0 (black circles) and $\mathcal{R}_{\text{max}}$ (red triangles) as a function of disorder strength for the data set in **a)**. **c):** Maximal response $\mathcal{R}_{\text{max}}$ versus timescale τ_0 for the diffusive (gray squares) and ballistic (open circles) cases. **d):** Thermoelectric response $\mathcal{R}$ in the regime of strong disorder from $\bar{V} = 542$ nK (gray circles) to 1220 nK (black diamonds) and fixed $\nu_z = 4.95$ kHz, in which the time dependence has been rescaled by τ_0. Black line: theoretical calculations.
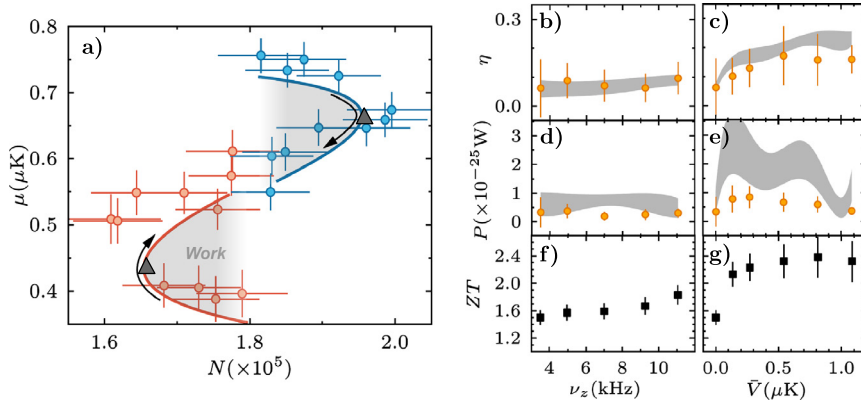

Fig. 5. Heat-to-work conversion, adapted from [27]. **a)** Thermodynamic cycle performed by the system in the μ–N plane for $\nu_z = 3.5$ kHz and $\bar{V} = 542$ nK. The evolution of the hot reservoir is depicted in red and that of the cold one in blue. The solid lines are given by the theory, and the black arrows indicate the direction of time. The two gray triangles indicate the turning points at which the conversion process ends. **b)**, **d)** Efficiency, power of the channel in the ballistic case, as a function of confinement. **c)**, **e)** The same quantities as functions of disorder strength for $\nu_z = 3.5$ kHz. Orange symbols: experiments; grey area: theory. **f)**, **g)** Dimensionless figure of merit ZT as a function of confinement and disorder for ballistic and diffusive channels, respectively.

process ends. The starting points have the same particle number, but, owing to the initial temperature imbalance, they have different chemical potentials. The latter is responsible for the 'reservoir' thermoelectric effect, which will tend to reduce the efficiency of the thermoelectric conversion performed in the junction. As in the case of a usual heat engine [41], the area enclosed by the cycle yields the total work. Strictly speaking, the conversion process ends at the turning point of the cycle, shown as dark gray triangles in Fig. 5a. Beyond that point, the system is essentially performing an equilibration of the particle number to restore thermodynamic equilibrium and behaves more like a discharging capacitor.

All the effective transport coefficients are ratios that depend only on the variable $\frac{\mu}{k_{\text{B}}T}$ or equivalently on T/T_{F}. The solutions to the evolution equations (6) also contain the entropy imbalance and the chemical potential difference as a function of time, which allows one to compute the efficiency of the thermoelectric process, defined as the ratio between the output chemical work performed during the whole cycle (including the decrease in the second stage) and the amount of entropy generated during the evolution. The expression for those two quantities is directly extracted from the force-flux formulation of out-of-equilibrium thermodynamics [36,35,41]:

$$\eta \equiv \frac{\text{Work}}{\text{Dissipated heat}} = -\frac{\int (\dot{N}_c - \dot{N}_h) \cdot (\mu_c - \mu_h)\,\mathrm{d}t}{\int (\dot{S}_c - \dot{S}_h) \cdot (T_c - T_h)\,\mathrm{d}t} = \frac{-\alpha\alpha_r}{\ell + L + \alpha^2 - \alpha\alpha_r} \tag{20}$$

The efficiency of the heat-to-work conversion is depicted in Fig. 5b–c in the ballistic and diffusive regimes, respectively. The corresponding output powers are displayed in Fig. 5d–e. They show that the efficiency is an increasing function of thermopower, as expected, and that the evolution of the efficiency is identical to that of the thermoelectric figure of merit ZT plotted in Fig. 5f–g. As expected from thermodynamic considerations, the slow dynamics induced by strong disorder implies a high efficiency, at the price of low power as seen in Fig. 5d and e. This compromise between efficiency and output
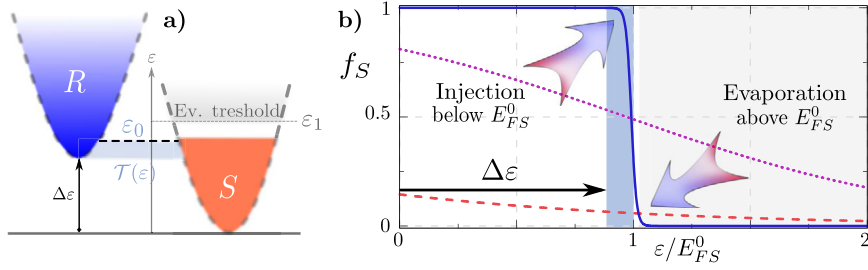
Fig. 6. Principle of Peltier cooling for cold atoms. **a)** Adapted from [48]. Sketch of the proposed Peltier cooling scheme: atoms are injected from deep energy levels of the reservoir cloud (R) into the system cloud (S) just below the Fermi level $E_{F,S}^{(0)}$ through a channel with an energy-dependent transmission $\mathcal{T}(\varepsilon)$. Additionally, the system is submitted to evaporative cooling with a fixed evaporation threshold ε_1 located above the Fermi level, removing high-energy particles, as indicated in the grey area above S. **b)** Evolution of the Fermi distribution of the system at three stages during the cooling process: initial (dashed red curve, $T_S \approx T_{FS}$), intermediate (purple dotted curve, $T_S = 0.3 T_{FS}$) and final (solid blue curve, $T_S = 0.02 T_{FS}$). The evolution, indicated by arrows, is calculated for $\varepsilon_1 = 1.05 E_{FS}^0$, $\gamma_{ev}\tau_0 = 1/16$, $\varepsilon_0 = 0.99 E_{FS}^0$, $\Delta\varepsilon = 0.96 E_{FS}^0$ and $E_{FS}^0 = 0.25 E_{FR}^0$, for an ideal sharp transmission (see below). The blue and grey shaded regions indicate the injection and evaporation energy windows, respectively.

power is at the heart of the discussion of thermoelectric energy conversion [42], and it is clear that the characterization of the thermoelectric performance of a material should be based on both the thermoelectric figure of merit and the power factor $G\alpha^2$.

This theory–experiment comparison assesses the potential of cold atoms for emulating thermal transport properties. From a broader perspective, those results also show that the quantum simulation trend in cold atoms is also valid for transport, and could then provide clues on the path to the realization of new materials with interesting energy saving properties. From the cold atoms perspective, this study of thermoelectric effects opens the way to control over heat transport with well-designed transport properties, which we proposed to use as a mean to overcome fundamental limitations in cooling processes.

3. Making cold atoms cooler

Low temperatures have been a long-standing quest in the cold atom community, especially for fermionic gases. The combination of laser cooling and evaporative cooling [43,44] has proved very efficient to reach temperatures sufficiently low to get quantum degenerate gases with entropy per particle as low as $T/T_F \approx 0.1$ [45]. Nevertheless, this typical value is still too high to rely on cold atoms to emulate many interesting quantum phases such as fractional quantum Hall systems [46], or to investigate the antiferromagnetic order in the Hubbard model [45,47,2].

In [48], we have proposed a cooling scheme for fermionic quantum gases, based on the principles of the Peltier effect, combined with evaporative cooling. We have shown that both a significantly lower entropy per particle and a faster cooling rate can be achieved compared to using only evaporative cooling.

3.1. A cold-atom Peltier module

Our proposal is inspired by the two terminal setups realized at ETH [18] discussed in the previous section. The proposed setup is displayed in Fig. 6a. The idea is to cool down one of the two clouds (the system S) with a technique based on thermoelectric effects [27–29,49–54] appearing at the junction between S and the second cloud (the reservoir R), which will ultimately be separated from the system. As its counterpart discussed in the previous section, the Peltier effect is a reversible thermoelectric phenomenon.

Both the reservoir R and the system S are prepared in harmonic traps, and their initial Fermi energies are $E_{F,R/S}^0 = h\bar{\nu}(3N_{R/S})^{1/3}$, with $\bar{\nu}$ the average trapping frequency and N_R, N_S the atom numbers. The reservoir and the system differ in their populations: $N_R > N_S$ (implying in particular that the ratio $T_R/T_{F,R}$ is lower than $T_S/T_{F,R}$ in the reservoir). Additionally, the lowest energy state of the reservoirs R is offset by $\Delta\varepsilon \geq 0$ against the lowest energy state of the system S. A 'junction' with an energy-dependent transmission connects the reservoir and the system in order to allow particle exchange in between the two. Within this setup, two different processes can lead to cooling. The first process is the usual evaporative cooling of the system in which hot atoms above the Fermi surface are removed from the gas. The second process is the filling in of holes below the Fermi surface of the system via the energy-resolved junction using atoms from the reservoir.

Our theoretical description of the cooling process relies on coupled rate equations [55–57,43] for the distribution functions f_S and f_R. The evolution is driven by the combined action of the junction between the reservoir and the system and the evaporation (which acts on the system only). The evolution of the thermodynamic quantities (particle number, energy and entropy in our case) in the two harmonic traps is quasistatic, provided that the thermalization is fast enough. This quite crucial assumption has been experimentally verified in the two terminal configuration of ETH, even in the case where many conduction channels are simultaneously open. Under this assumption, the particle current leaving the reservoir, given by
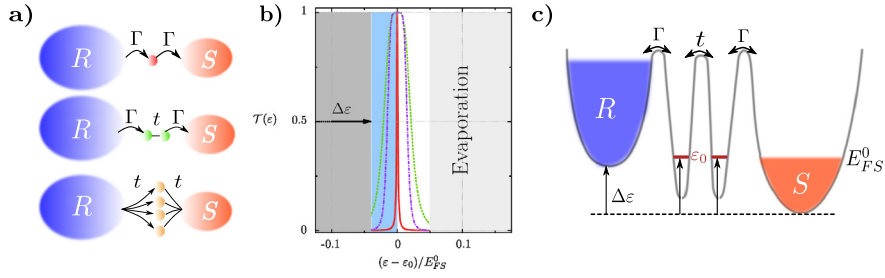
Fig. 7. a) Sketches of the different propositions to realize the desired energy-dependent transmission functions. Top (red dot): a single resonant level, with a transmission given by (24). Middle (green dots): two resonant levels in series connected by a tunneling probability, generating a transmission given by (25). Bottom (orange dots): several resonant levels in parallel. **b)** Adapted from [48]. The corresponding energy-dependent transmission coefficients, plotted for parameters identical to those in Fig. 8. The light grey area indicates states above ε_1, which are subject to evaporation, while the dark grey one indicates those below $\Delta\varepsilon$, which do not participate in transport. The light blue area corresponds to the ideal box-like transmission, bounded by the band bottom and ε_0. The transmission for three resonant levels in series is shown in purple for comparison with that of the two levels in series. **c)** Sketch of the energy levels for two resonant levels in series.

the Landauer formula, can be directly related to the variation of the particle number in the reservoirs, to give the following coupled evolution of the two distribution functions:

$$g_R(\varepsilon)\frac{\mathrm{d}f_R(\varepsilon)}{\mathrm{d}t} = -\frac{\mathcal{T}(\varepsilon)}{h}[f_R - f_S](\varepsilon) \tag{21}$$

$$g_S(\varepsilon)\frac{\mathrm{d}f_S(\varepsilon)}{\mathrm{d}t} = \frac{\mathcal{T}(\varepsilon)}{h}[f_R - f_S](\varepsilon) - \Gamma_{\mathrm{ev}}(\varepsilon)g_S(\varepsilon)f_S(\varepsilon) \tag{22}$$

where $g_{S,R}$ are the densities of states in the system and reservoir. Unless specified, the number of transport channels is one, such that the transport function representing the connection between the system and reservoir reduces to the energy dependent transmission $\mathcal{T}(\varepsilon)$, which we propose to tune to improve the cooling power. Let us note that since $\mathcal{T}(\varepsilon)$ is dimensionless, the typical timescale that rules the time-evolution in these equations is $\tau_0 = hg_S(E_{FS}^0) = h\left(E_{FS}^0\right)^2/3(h\bar{\nu})^3$, in agreement with the relevant timescale for the particle transport identified previously [18,27]. The effect of evaporation, acting on the system only, has been included as a leak of high-energy particles above a fixed energy threshold ε_1, with an energy independent rate $\Gamma_{\mathrm{ev}}(\varepsilon) = \gamma_{\mathrm{ev}}\vartheta(\varepsilon - \varepsilon_1)$ [43], with ϑ the Heaviside step function. Excluding the trapping geometry, the parameters at hand include the energy bias $\Delta\varepsilon$, the typical transmission energy ε_0 and the evaporation threshold ε_1. In [48], we performed a systematic exploration of the parameter space for different transmissions, monitoring the evolution of the entropy per particle, particle number and energy as a function of time.

3.2. Fast and efficient cooling with Peltier and evaporation

A good benchmark for a cooling protocol relies on two criteria. The first one is to reach the best cooling efficiency in the sense of thermodynamics: in analogy with usual cooling processes [41], this means reaching the lowest possible entropy per particle. However, in practice one needs to take into account the speed at which the cooling operation is performed, since in experiments other destructive processes may be present, such as heating processes by the interaction with the applied trapping lasers or scattering with the thermal background gas. Therefore, it is important to make sure that the *rate* at which atoms are cooled is high enough to overcome the heating rate imposed by the experimental setup. Thus, a good cooling protocol must be powerful and thermodynamically efficient at the same time. Consequently, we have calculated the cooling rate defined as the amount of entropy per particle s removed per unit time:

$$\eta\,\tau_0 = \frac{\mathrm{d}s}{\mathrm{d}t} \tag{23}$$

In the context of solid-state devices, an energy-resolved transmission of a resonant level (Eq. (24) below) has been shown [58] to enhances thermopower, and to improve drastically the efficiency of the heat-to-particle current conversion. Nevertheless, a good cooling efficiency does not ensure a good cooling power, which depends on the power factor $\alpha^2 G$. The study performed in [59] showed that optimizing the power factor instead of the thermoelectric figure of merit ZT actually leads to a box-like transmission (Eq. (26) below), which can be mimicked with resonant levels in series (Eq. (25) below). Optimizing the power factor instead of the figure of merit is equivalent to optimize power instead of efficiency. Starting from these considerations, we have compared the efficiency and cooling power of the following three transmissions, which are also shown in Fig. 7, together with possible experimental implementations:

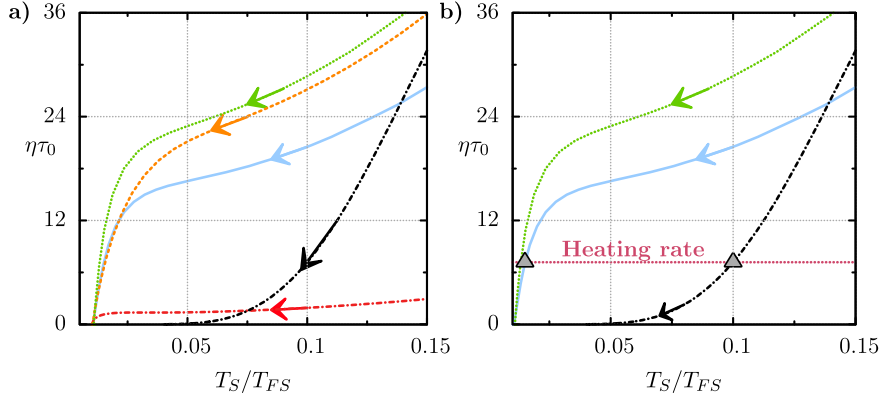$$\mathcal{T}_{1RL}(\varepsilon) = \frac{\Gamma^2}{(\varepsilon - \varepsilon_0)^2 + \Gamma^2} \tag{24}$$

Fig. 8. Adapted from [48]. **a)** Dimensionless cooling rate $\eta(t)\,\tau_0$ as a function of T_S/T_{FS}, for $\Delta\varepsilon = 0.96\,E_{FS}^0$ and various transmissions centered at $\varepsilon_0 = 0.99\,E_{FS}^0$, and $E_{FS}^0/E_{FR}^0 = 1/4$, $\varepsilon_1 = 1.05\,E_{FS}^0$, $\gamma_{ev}\tau_0 = 15$, $\Delta\varepsilon = 0.96\,E_{FS}^0$: The (red) dot-dashed and (orange) dashed curves correspond to a single and 100 parallel resonant level(s), respectively, with $\Gamma = 1\cdot 10^{-3}\,E_{FS}^0$. The (green) dotted curve is for two resonant levels in series of width $\Gamma = 0.03\,E_{FS}^0$ and the (light blue) solid curve is for an ideal box transmission. (Black) dashed-dotted curve shows the evaporative cooling only. **b)** Dimensionless cooling rate as a function of the entropy per particle, for the same parameter values as in **a)**. The arrows indicate the direction of time evolution. The horizontal (red) dotted line indicates a typical heating rate limiting these cooling processes. The gray triangles signal the end of the cooling process, defined as the intersection of the curves with the horizontal line accounting for the heating rate.

$$\mathcal{T}_{2RL}(\varepsilon) = \frac{\Gamma^2 t^2}{\left[(\varepsilon - \varepsilon_0)^2 + \Gamma^2/4 - t^2\right]^2 + \Gamma^2 t^2} \tag{25}$$

$$\mathcal{T}_{\text{box}} = \vartheta(\varepsilon - \varepsilon_0) \tag{26}$$

The cooling rates obtained for the different transmissions are depicted in Fig. 8a. They show in particular that the resonant levels in series or in parallel satisfy both criteria: they offer a good cooling rate, and they allow one to obtain a rather low final entropy per particle. As expected, the results for the single resonant level are pretty good in terms of the final entropy per particle, but the associated rate is rather poor, since the current passing through the single level cannot compensate efficiently the evaporation losses. Also, the result obtained with the resonant levels in parallel is even better than that obtained with the ideal box transmission, which can be attributed to the extra current going through the tails of the transmission function, which makes it more efficient at the initial cooling stage. Fig. 8b displays the cooling rate for the ideal box transmission and for single evaporation, together with a phenomenological heating rate, which signals the end of the cooling process, chosen such that evaporative cooling allows one to obtain a temperature of $0.1\,T_F$ approximately. Under the same conditions, the Peltier cooling scheme allows to reach temperatures as low as $0.015\,T_F$.

In addition, the results for the evolution of the particle number are represented in Fig. 9 for an ideal box-like transmission, showing that, in contrast to evaporative cooling, our cooling proposal is not accompanied by particle losses. The losses due to evaporation are overcompensated by particles from the reservoirs, in the sense that we propose to trade high-energy particles for low-energy ones: from this point of view, our cooling scheme can be understood as the simultaneous evaporation of particles and holes at fixed Fermi energy, thus performing a control on entropy transport, leading to a rectification of the distribution function in the reservoirs, as displayed in Fig. 6. The inset in Fig. 9 confirms that the poor results obtained with the single resonant level come from the difficulties to compensate for the particle losses. The resonant levels in parallel and those in series perform similarly to the ideal box-like transmission.

4. Conclusion and perspectives

We have demonstrated in [27] that thermal and thermoelectric transport measurements can be performed in cold atomic gases, and that they are sensitive observables, complementary to a conductance measurement.

Elaborating on this theory-experiment confrontation, we have proposed [48] a fast and efficient cooling scheme for fermionic gases based on evaporation and energy-selective injection of particles. This proposal can be readily implemented with state-of-the-art projection techniques [60], and appears as a plausible answer to a long-standing goal of low temperatures with cold fermionic gases.

Owing to the control on interactions via Feshbach resonances, the experimental technique developed in [27] can be generalized to strongly interacting systems where thermoelectric properties are of fundamental interest [61–63]. Entering the correlated regime would make the setup an interesting controllable testbed for theories on the transport properties of strongly interacting systems [64], and it would be of great interest to extend the existing results on particle transport [23,26] to thermal and thermoelectric properties, which appear as efficient probes of the excitations of a system, as opposed to the particle current, which contains contributions stemming also from the ground state. Thus, extending both the theoretical and experimental results presented in the first part to the strongly interacting limit of the Hubbard model would be a milestone to the quantum simulation of purely out-of-equilibrium properties of strongly correlated models. As an example,
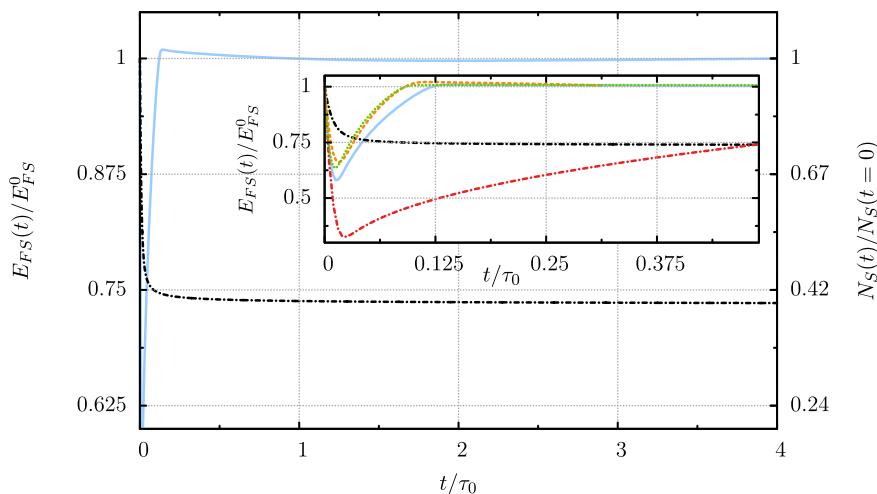
Fig. 9. Adapted from [48]: The system's Fermi energy $E_{FS}(t)$ (left axis) and particle number $N_S(t)$ (right axis). The solid light blue curve is for the Peltier cooling with $E_{FS}^0/E_{FR}^0 = 1/4$ and $\varepsilon_1 = 1.05\,E_{FS}^0$, $\gamma_{ev}\tau_0 = 15$, $\varepsilon_0 = 0.99\,E_{FS}^0$, $\Delta\varepsilon = 0.96\,E_{FS}^0$. The dashed-dotted black curve is for evaporative cooling only, with an initial particle number $N = N_S + N_R$ and $\varepsilon_1 = 1.05\,E_F$. **Inset:** Comparison between the different realizations at short times. The parameters are the same as in Fig. 8.

investigating the mechanisms responsible for energy exchanges in the strongly interacting, insulating phase of the Hubbard model allowing for the relaxation of a temperature imbalance would give an insight into genuine many-body effects out of the ground state. Characterizing those mechanisms remains a challenging question, both theoretically and experimentally, and any opportunity to investigate them should be taken. Along the same lines, exploring attractive interactions would reveal the physics of excitations of strongly correlated superfluids, and draw a relation between second sound (and more generally thermomechanical effects) and thermoelectricity as entropy conveyors.

The recent emergence of periodic driving techniques in cold atomic systems [65] also offer interesting perspectives to simulate AC thermopower.

Acknowledgements

References

[1] R.P. Feynman, Simulating physics with computers, Int. J. Theor. Phys. 21 (6) (1982) 467–488.

[2] I. Bloch, J. Dalibard, W. Zwerger, Many-body physics with ultracold gases, Rev. Mod. Phys. 80 (2008) 885–964, http://dx.doi.org/10.1103/RevModPhys. 80.885.

[3] I. Bloch, J. Dalibard, S. Nascimbene, Quantum simulations with ultracold quantum gases, Nat. Phys. 8 (4) (2012) 267–276.

[4] M. Lewenstein, A. Sanpera, V. Ahufinger, Ultracold Atoms in Optical Lattices: Simulating Quantum Many-Body Systems, OUP, Oxford, 2012, http://books. google.es/books?id=Wpl91RDxV5IC.

[5] J. Catani, G. Lamporesi, D. Naik, M. Gring, M. Inguscio, F. Minardi, A. Kantian, T. Giamarchi, Quantum dynamics of impurities in a one-dimensional Bose gas, Phys. Rev. A 85 (2012) 023623, http://dx.doi.org/10.1103/PhysRevA.85.023623.

[6] S. Palzer, C. Zipkes, C. Sias, M. Köhl, Quantum transport through a Tonks–Girardeau gas, Phys. Rev. Lett. 103 (2009) 150601, http://dx.doi.org/10.1103/ PhysRevLett.103.150601.

[7] J.H. Thywissen, R.M. Westervelt, M. Prentiss, Quantum point contacts for neutral atoms, Phys. Rev. Lett. 83 (1999) 3762–3765, http://dx.doi.org/10.1103/ PhysRevLett.83.3762.

[8] H. Ott, E. de Mirandes, F. Ferlaino, G. Roati, G. Modugno, M. Inguscio, Collisionally induced transport in periodic potentials, Phys. Rev. Lett. 92 (2004) 160601, http://dx.doi.org/10.1103/PhysRevLett.92.160601.

[9] J. Billy, V. Josse, Z. Zuo, A. Bernard, B. Hambrecht, P. Lugan, D. Clément, L. Sanchez-Palencia, P. Bouyer, A. Aspect, Direct observation of Anderson localization of matter waves in a controlled disorder, Nature 453 (7197) (2008) 891–894.

[10] G. Roati, C. D'Errico, L. Fallani, M. Fattori, C. Fort, M. Zaccanti, G. Modugno, M. Modugno, M. Inguscio, Anderson localization of a non-interacting Bose–Einstein condensate, Nature 453 (7197) (2008) 895–898.

[11] S.S. Kondov, W.R. McGehee, J.J. Zirbel, B. DeMarco, Three-dimensional Anderson localization of ultracold matter, Science 334 (6052) (2011) 66–68, http://dx.doi.org/10.1126/science.1209019., http://www.sciencemag.org/content/334/6052/66.abstract.

[12] K.K. Das, S. Aubin, Quantum pumping with ultracold atoms on microchips: fermions versus bosons, Phys. Rev. Lett. 103 (2009) 123007, http://dx.doi.org/ 10.1103/PhysRevLett.103.123007.

[13] M. Schreiber, S.S. Hodgman, P. Bordia, H.P. Lüschen, M.H. Fischer, R. Vosk, E. Altman, U. Schneider, I. Bloch, Observation of many-body localization of interacting fermions in a quasirandom optical lattice, Science 349 (6250) (2015) 842–845.

[14] A. Ramanathan, K.C. Wright, S.R. Muniz, M. Zelan, W.T. Hill, C.J. Lobb, K. Helmerson, W.D. Phillips, G.K. Campbell, Superflow in a toroidal Bose–Einstein condensate: an atom circuit with a tunable weak link, Phys. Rev. Lett. 106 (2011) 130401.

[15] S. Eckel, J.G. Lee, F. Jendrzejewski, N. Murray, C.W. Clark, C.J. Lobb, W.D. Phillips, M. Edwards, G.K. Campbell, Hysteresis in a quantized superfluid 'atomtronic' circuit, Nature 506 (7487) (2014) 200–203.

[16] B.T. Seaman, M. Krämer, D.Z. Anderson, M.J. Holland, Atomtronics: ultracold-atom analogs of electronic devices, Phys. Rev. A 75 (2007) 023615, http://dx.doi.org/10.1103/PhysRevA.75.023615.

[17] Focus on atomtronics and quantum technologies, New J. Phys. (2016), http://iopscience.iop.org/1367-2630/focus/Focus%20on%20Atomtronics-enabled%20Quantum%20Technologies.

[18] J.-P. Brantut, J. Meineke, D. Stadler, S. Krinner, T. Esslinger, Conduction of ultracold fermions through a mesoscopic channel, Science 337 (6098) (2012) 1069–1071, http://dx.doi.org/10.1126/science.1223175, http://www.sciencemag.org/content/337/6098/1069.abstract.

[19] S. Krinner, D. Stadler, D. Husmann, J.-P. Brantut, T. Esslinger, Observation of quantized conductance in neutral matter, Nature 517 (7532) (2015) 64–67.

[20] M. Bruderer, W. Belzig, Mesoscopic transport of fermions through an engineered optical lattice connecting two reservoirs, Phys. Rev. A 85 (2012) 013623, http://dx.doi.org/10.1103/PhysRevA.85.013623.

[21] T. Sekera, C. Bruder, W. Belzig, Thermoelectricity in a junction between interacting cold atomic Fermi gases, Phys. Rev. A 94 (2016) 033618.

[22] D. Stadler, S. Krinner, J. Meineke, J.-P. Brantut, T. Esslinger, Observing the drop of resistance in the flow of a superfluid Fermi gas, Nature 491 (7426) (2012) 736–739.

[23] D. Husmann, S. Uchino, S. Krinner, M. Lebrat, T. Giamarchi, T. Esslinger, J.-P. Brantut, Connecting strongly correlated superfluids by a quantum point contact, Science 350 (6267) (2015) 1498–1501.

[24] S. Krinner, D. Stadler, J. Meineke, J.-P. Brantut, T. Esslinger, Superfluidity with disorder in a thin film of quantum gas, Phys. Rev. Lett. 110 (2013) 100601, http://dx.doi.org/10.1103/PhysRevLett.110.100601.

[25] S. Krinner, D. Stadler, J. Meineke, J.-P. Brantut, T. Esslinger, Observation of a fragmented, strongly interacting Fermi gas, Phys. Rev. Lett. 115 (2015) 045302, http://dx.doi.org/10.1103/PhysRevLett.115.045302.

[26] S. Krinner, M. Lebrat, D. Husmann, C. Grenier, J.-P. Brantut, T. Esslinger, Mapping out spin and particle conductances in a quantum point contact, Proc. Natl. Acad. Sci. USA (2016) 201601812.

[27] J.-P. Brantut, C. Grenier, J. Meineke, D. Stadler, S. Krinner, C. Kollath, T. Esslinger, A. Georges, A thermoelectric heat engine with ultracold atoms, Science 342 (6159) (2013) 713–715, http://dx.doi.org/10.1126/science.1242308, http://www.sciencemag.org/content/342/6159/713.abstract.

[28] C. Grenier, C. Kollath, A. Georges, Probing thermoelectric transport with cold atoms, arXiv:1209.3942, 2012.

[29] E.L. Hazlett, L.-C. Ha, C. Chin, Anomalous thermoelectric transport in two-dimensional Bose gas, arXiv:1306.4018.

[30] A. Rançon, C. Chin, K. Levin, Bosonic thermoelectric transport and breakdown of universality, New J. Phys. 16 (11) (2014) 113072, http://stacks.iop.org/1367-2630/16/i=11/a=113072.

[31] D. MacDonald, Thermoelectricity: An Introduction to the Principles, Dover Books on Physics, Dover Publications, 2006.

[32] S. Datta, Electronic Transport in Mesoscopic Systems, Cambridge Studies in Semiconductor Physics and Microelectronic Engineering, Cambridge University Press, Cambridge, UK, 1997, http://books.google.fr/books?id=28BC-ofEhvUC.

[33] Y. Imry, Introduction to Mesoscopic Physics, Mesoscopic Physics and Nanotechnology, Oxford University Press, Oxford, UK, 2008.

[34] H.J. Goldsmid, Introduction to Thermoelectricity, Springer Series in Materials Science, Springer, Dordrecht, the Netherlands, 2009.

[35] L. Onsager, Reciprocal relations in irreversible processes. I, Phys. Rev. 37 (1931) 405–426, http://dx.doi.org/10.1103/PhysRev.37.405.

[36] L. Onsager, Reciprocal relations in irreversible processes. II, Phys. Rev. 38 (1931) 2265–2279, http://dx.doi.org/10.1103/PhysRev.38.2265.

[37] N. Ashcroft, N. Mermin, Solid State Physics, Saunders College, Philadelphia, PA, USA, 1976.

[38] A. Staring, L. Molenkamp, B. Alphenaar, H. Van Houten, O. Buyk, M. Mabesoone, C. Beenakker, C. Foxon, Coulomb-blockade oscillations in the thermopower of a quantum dot, Europhys. Lett. 22 (1) (1993) 57.

[39] L. Hicks, M. Dresselhaus, Effect of quantum-well structures on the thermoelectric figure of merit, Phys. Rev. B 47 (19) (1993) 12727.

[40] L. Hicks, M. Dresselhaus, Thermoelectric figure of merit of a one-dimensional conductor, Phys. Rev. B 47 (24) (1993) 16631.

[41] H.B. Callen, Thermodynamics, John Wiley & Sons, Inc., New York, 1960.

[42] F. Curzon, B. Ahlborn, Efficiency of a Carnot engine at maximum power output, Am. J. Phys. 43 (1) (1975) 22–24.

[43] W. Ketterle, N. van Druten, Evaporative cooling of trapped atoms, Adv. At. Mol. Opt. Phys. 37 (1996) 181.

[44] C.J. Pethick, H. Smith, Bose–Einstein Condensation in Dilute Gases, 2nd edition, Cambridge University Press, Cambridge, UK, 2008, http://www.amazon.com/exec/obidos/redirect?tag=citeulike07-20&path=ASIN/052184651X.

[45] D.C. McKay, B. DeMarco, Cooling in strongly correlated optical lattices: prospects and challenges, Rep. Prog. Phys. 74 (5) (2011) 054401, http://stacks.iop.org/0034-4885/74/i=5/a=054401.

[46] N. Cooper, Rapidly rotating atomic gases, Adv. Phys. 57 (6) (2008) 539–616, http://dx.doi.org/10.1080/00018730802564122.

[47] R. Jördens, L. Tarruell, D. Greif, T. Uehlinger, N. Strohmaier, H. Moritz, T. Esslinger, L. De Leo, C. Kollath, A. Georges, V. Scarola, L. Pollet, E. Burovski, E. Kozik, M. Troyer, Quantitative determination of temperature in the approach to magnetic order of ultracold fermions in an optical lattice, Phys. Rev. Lett. 104 (2010) 180401, http://dx.doi.org/10.1103/PhysRevLett.104.180401.

[48] C. Grenier, A. Georges, C. Kollath, Peltier cooling of fermionic quantum gases, Phys. Rev. Lett. 113 (2014) 200601, http://dx.doi.org/10.1103/PhysRevLett.113.200601.

[49] D.J. Papoular, G. Ferrari, L.P. Pitaevskii, S. Stringari, Increasing quantum degeneracy by heating a superfluid, Phys. Rev. Lett. 109 (2012) 084501, http://dx.doi.org/10.1103/PhysRevLett.109.084501.

[50] D.J. Papoular, L.P. Pitaevskii, S. Stringari, Fast thermalization and Helmholtz oscillations of an ultracold Bose gas, Phys. Rev. Lett. 113 (2014) 170601, http://dx.doi.org/10.1103/PhysRevLett.113.170601.

[51] L.A. Sidorenkov, M.K. Tey, R. Grimm, Y.-H. Hou, L. Pitaevskii, S. Stringari, Second sound and the superfluid fraction in a Fermi gas with resonant interactions, Nature 498 (7452) (2013) 78–81.

[52] H. Kim, D.A. Huse, Heat and spin transport in a cold atomic Fermi gas, Phys. Rev. A 86 (5) (2012) 053607, http://dx.doi.org/10.1103/PhysRevA.86.053607.

[53] C.H. Wong, H.T.C. Stoof, R.A. Duine, Spin-Seebeck effect in a strongly interacting Fermi gas, Phys. Rev. A 85 (2012) 063613, http://dx.doi.org/10.1103/PhysRevA.85.063613.

[54] T. Karpiuk, B. Grémaud, C. Miniatura, M. Gajda, Superfluid fountain effect in a Bose–Einstein condensate, Phys. Rev. A 86 (2012) 033619, http://dx.doi.org/10.1103/PhysRevA.86.033619.

[55] O.J. Luiten, M.W. Reynolds, J.T.M. Walraven, Kinetic theory of the evaporative cooling of a trapped gas, Phys. Rev. A 53 (1996) 381–389, http://dx.doi.org/10.1103/PhysRevA.53.381.

[56] K. Davis, M.-O. Mewes, W. Ketterle, An analytical model for evaporative cooling of atoms, Appl. Phys. B 60 (2–3) (1995) 155–159, http://dx.doi.org/10.1007/BF01135857.

[57] H. Metcalf, P. van der Straten, Laser Cooling and Trapping, Graduate Texts in Contemporary Physics, Springer, New York, 1999, http://books.google.ch/books?id=i-40VaXqrj0C.

[58] G.D. Mahan, J.O. Sofo, The best thermoelectric, Proc. Natl. Acad. Sci. USA 93 (15) (1996) 7436–7439, http://www.pnas.org/content/93/15/7436.abstract.

[59] R.S. Whitney, Most efficient quantum thermoelectric at finite power output, Phys. Rev. Lett. 112 (2014) 130601, http://dx.doi.org/10.1103/PhysRevLett.112.130601.

[60] B. Zimmermann, T. Müller, J. Meineke, T. Esslinger, H. Moritz, High-resolution imaging of ultracold fermions in microscopically tailored optical potentials, New J. Phys. 13 (4) (2011) 043007, http://stacks.iop.org/1367-2630/13/i=4/a=043007.

[61] K. Behnia, D. Jaccard, J. Flouquet, On the thermoelectricity of correlated electrons in the zero-temperature limit, J. Phys. Condens. Matter 16 (28) (2004) 5187.

[62] X. Zhang, C.-L. Hung, S.-K. Tung, N. Gemelke, C. Chin, Exploring quantum criticality based on ultracold atoms in optical lattices, New J. Phys. 13 (4) (2011) 045011.

[63] T. Micklitz, A. Levchenko, A. Rosch, Nonlinear conductance of long quantum wires at a conductance plateau transition: where does the voltage drop?, Phys. Rev. Lett. 109 (2012) 036405.

[64] P.M. Chaikin, G. Beni, Thermopower in the correlated hopping regime, Phys. Rev. B 13 (1976) 647–651, http://dx.doi.org/10.1103/PhysRevB.13.647.

[65] G. Jotzu, M. Messer, R. Desbuquois, M. Lebrat, T. Uehlinger, D. Greif, T. Esslinger, Experimental realization of the topological Haldane model with ultracold fermions, Nature 515 (7526) (2014) 237–240.